Modeling the Inertial Torque Imbalance Within an Internal Combustion Engine: Quantifying the Equivalent Mass Approximation

Noah D. Manring
Mechanical and Aerospace Engineering,
University of Missouri,
Columbia, MO 65211
e-mail: ManringN@missouri.edu

Muslim Ali
Mechanical and Aerospace Engineering,
University of Missouri,
Columbia, MO 65211
e-mail: mma26b@mail.missouri.edu

The objectives of this research are to explore the inertial-torque characteristics of an inline, internal combustion engine with connecting-rod joints that are evenly spaced about the centerline of the crankshaft, and to evaluate the goodness of a mass approximation that is customarily used in machine design textbooks. In this research, the number of pistons within the internal combustion engine is varied from 1 to 8. In order to generalize the results, the inertial-torque equations are nondimensionalized and shown to depend upon only four nondimensional groups, all related to the mass and geometry properties of the connecting rod. As shown in this research, the inertial-torque imbalance is greatest for an engine with two pistons, and that a dramatic reduction in the torque imbalance may be obtained for engine designs that use four or more pistons. It is also shown in this paper that the customary mass approximations for the connecting rod may be used to simplify the analysis for all engine designs without a significant loss of modeling accuracy. [DOI: 10.1115/1.4039282]

Introduction

Background. The inertia of moving parts within an internal combustion engine produces an imbalance of forces and moments that must be absorbed by the engine foundation. The absorbing of these forces and moments produces a shaking effect for the engine that is undesirable, and therefore, engine designers have made great efforts to balance the engine by designing inertia properties that ideally cancel themselves out. An internal combustion engine uses a slider–crank mechanism to displace each reciprocating piston and to convert linear mechanical-power into rotational mechanical-power at the crankshaft. Although the geometry of the slider–crank mechanism appears to be straightforward and simple—two right triangles always sharing a common side—analysts have nevertheless felt compelled to simplify the inertia problem for the engine by using an equivalent mass approximation which lumps the mass of the connecting rod at each end while producing a mass moment-of-inertia that is not necessarily equal to that of the actual connecting rod [1–4]. This has been done to simplify the mechanical analysis since the kinematic properties of both ends of the connecting rod are well known; however, the validity of making this approximation has not been established in the literature by a rigorous comparison between the actual and the approximate model. Even with such a simplifying assumption, however, it has been shown that the inertial torque acting on the crank shaft can never be entirely eliminated by any kind of balancing for reasonable engine designs [4]. As a result of this fact, adverse vibration effects have been reduced by the proper selection of mountings and vibration absorbers [5–7]. Furthermore, while the single-piston engine has been studied at length, the total magnitude of the inertial imbalance has not been presented in the literature for multipiston designs. This paper aims to address these deficiencies.

Contributed by the Dynamic Systems Division of ASME for publication in the Journal of Dynamic Systems, Measurement, and Control. Manuscript received January 10, 2017; final manuscript received October 31, 2017; published online March 28, 2018. Assoc. Editor: Douglas Bristow.

Literature Review. As previously noted, machine design textbooks have routinely modified the connecting rod mass properties for the internal combustion engine in order to simplify the calculation of those for the inertial torque imbalance [1–4]. While this simplification is frequently applied, none of these textbooks discuss the validity of making this simplification. Within the literature, there is research that has been done to control the idle speed of the engine by seeking to balance the torque on the crankshaft using feedback control methods [8,9]. This work appears to neglect the inertial imbalance explicitly, considering the primary source of imbalance during idle to be related to the ignition of gas within a multipiston engine design. Other researchers have recognized the difficulty in eliminating the inertial torque imbalance that is inherent within the internal combustion engine, and they have put forward novel suggestions on how to handle this imbalance. For instance, Arakelian and Briot [10] have identified a design with offset mass and spring mechanisms attached to a cam-follower which is activated by the rotation of the crankshaft. As noted by others, this device is novel but not overly practical. An earlier work by Bagci [11] has put forward suggestions on how to counteract the inertial imbalance by strategically placing masses within the machine, but these suggestions also suffer from a lack of practicality when it comes to packaging an engine within a reasonable envelop of space. In these samples of literature, there has been no indication that anyone has quantified the magnitude of the inertial imbalance as it varies with the number of pistons that are used to design the machine. And it is certain that no one has compared the actual torque imbalance with the simplified calculations that are offered through equivalent mass models. In this paper, we attempt to do both of these things.

Objectives. The objectives of this research are to explore the inertial-torque characteristics of an inline, internal combustion engine with connecting-rod joints that are evenly spaced about the centerline of the crankshaft, and to evaluate the goodness of a mass approximation that is customarily used in machine design textbooks. In this research, the number of pistons within the

internal combustion engine is varied from 1 to 8. In order to generalize the results, the inertial-torque equations are nondimensionalized and shown to depend upon only four nondimensional groups, all related to the mass and geometry properties of the connecting rod. As shown in this research, the inertial-torque imbalance is greatest for an engine with two pistons, and that a dramatic reduction in the torque imbalance may be obtained for engine designs that use four or more pistons. It is also shown in this paper that the customary mass approximations for the connecting rod may be used to simplify the analysis for all engine designs without a significant loss of modeling accuracy.

Descriptions

Figure 1 shows a schematic of an inline, internal combustion engine that uses four pistons. In this figure, the connecting rods for the pistons are evenly spaced in a circular array about the centerline of the crankshaft and a torque T is applied to the crank in order to rotate the engine at a constant velocity shown by the symbol ω. This figure is presented to illustrate the inline configuration with evenly spaced connecting rods. The analysis that follows will consider an engine with up to eight pistons with evenly spaced connecting rods.

Figure 2 shows a schematic of a single piston within an internal combustion engine. This device is the classical four-bar, slider–crank mechanism used in many machines. The crank is shown in the figure by the dimension L_1 with the mass center of the crank located by the dimension r_1. The connecting rod is shown by the dimension L_2 and its mass center is located by the dimension r_2. The piston is shown by the box which is constrained to slide along the fixed surface. The mass center for the piston relative to the pin joint of the connecting rod is located by the dimension r_3. As the crank rotates in the direction shown by θ, the linear position of the piston x changes in a reciprocating manner. During this motion, the angular position of the connecting rod φ swings back and forth across the centerline of the piston and stays near zero for the case where $L_2 \gg L_1$. Since this paper focuses on the inertia of the reciprocating engine, the input force to the piston due to the pressure of ignited fuel is not included in Fig. 2. The torque required to rotate the crank at a constant angular velocity is shown in Fig. 2 by the symbol T. In this figure, the mass of the crank, the connecting rod, and the piston are shown by the symbols m_1, m_2, and m_3, respectively. The mass moment-of-inertia for the crank and the connecting rod about their mass centers is shown in Fig. 2 by the symbols I_1 and I_2, respectively.

Mechanical Analysis

General. In the following analysis, the mechanical operation of the reciprocating piston shown in Fig. 2 will be studied using standard methods of kinematic and kinetic analysis. The geometry of Fig. 2 will be used for kinematic analysis, while the free-body diagrams shown in Fig. 3 will be used for kinetic analysis.

Kinetic Analysis. In order to perform the kinetic analysis of the slider–crank mechanism shown in Fig. 2, the free-body diagrams for each linkage in the device must be studied. These free-body diagrams are shown in Fig. 3 for the crank, connecting rod, and piston.

Summing forces and moments on the free-body diagram in Fig. 3 for the crank produces the following equations of motion for this member:

$$\begin{aligned} m_1\, a_{1_x} &= F_{A_x} + F_{B_x} \\ m_1\, a_{1_y} &= F_{A_y} + F_{B_y} \\ 0 &= F_{A_x}\, r_1\, \sin(\theta) - F_{A_y}\, r_1\, \cos(\theta) - F_{B_x}\, (L_1 - r_1)\, \sin(\theta) \\ &\quad + F_{B_y}\, (L_1 - r_1)\, \cos(\theta) + T \end{aligned} \tag{1}$$

where a_{1_x} and a_{1_y} are, respectively, the instantaneous accelerations in the horizontal and vertical directions for the mass center of the crank relative to a Newtonian reference frame, F_{A_x} and F_{A_y} are the reaction forces acting on the crank at point A, F_{B_x} and F_{B_y} are the reaction forces acting on the crank at point B, and T is the torque exerted on the crank itself. Note: in the third equation of Eq. (1), which is the angular momentum equation, it is assumed that the rotational speed of the crankshaft ω is constant.

Similarly, summing the forces and moments on the free-body diagram in Fig. 3 for the connecting rod produces the following equations of motion for this member:

$$\begin{aligned} m_2\, a_{2_x} &= F_{C_x} - F_{B_x} \\ m_2\, a_{2_y} &= F_{C_y} - F_{B_y} \\ -I_2\, \ddot{\varphi} &= F_{C_x}\, r_2\, \sin(\varphi) + F_{C_y}\, r_2\, \cos(\varphi) \\ &\quad + F_{B_x}\, (L_2 - r_2)\, \sin(\varphi) + F_{B_y}\, (L_2 - r_2)\, \cos(\varphi) \end{aligned} \tag{2}$$

where a_{2_x} and a_{2_y} are, respectively, the instantaneous accelerations in the horizontal and vertical directions for the mass center of the connecting rod relative to a Newtonian reference frame, and F_{C_x} and F_{C_y} are the reaction forces acting on the crankshaft at point C.

Finally, summing forces and moments on the free-body diagram in Fig. 3 for the piston produces the following equations of motion for this member:

$$m_3\, \ddot{x} = -F_{C_x}, \quad 0 = -F_{C_y} + W, \quad 0 = F_{C_y}\, r_3 + W\, d \tag{3}$$

where W is the reaction force of the piston against the sidewall of the engine and d is the instantaneous location for this reaction force.

Equations (1)–(3) represent nine independent equations which may be used to solve for nine unknowns. Assuming that the kinematics of the crank are given, the list of nine unknowns that may be solved include F_{A_x}, F_{A_y}, F_{B_x}, F_{B_y}, T, F_{C_x}, F_{C_y}, W, and d. For the purposes of this research, we are only interested in the torque exerted on the crank at point A. Using the previous analysis, this result is given by

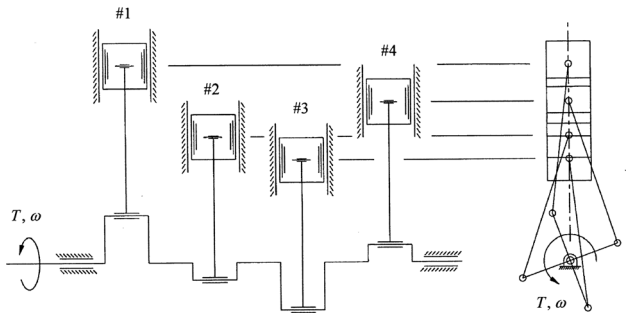

Fig. 1 A schematic of an inline, internal combustion engine using four pistons

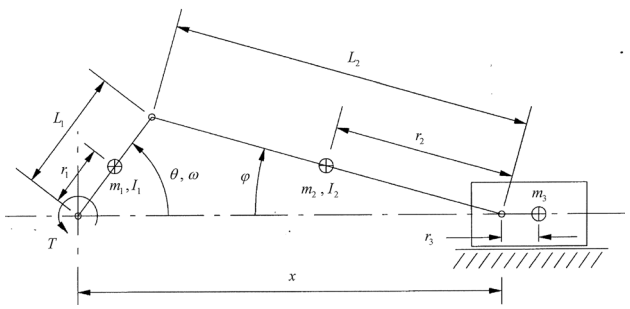

Fig. 2 A schematic of a single piston within the inline, internal combustion engine

$$T = m_2 L_1 \left(-\left[\sin(\theta) + \left(1 - \frac{r_2}{L_2} \right) \cos(\theta) \tan(\varphi) \right] a_{2_x} + \frac{r_2}{L_2} \cos(\theta)\, a_{2_y} \right) + I_2 \frac{L_1}{L_2} \frac{\cos(\theta)}{\cos(\varphi)} \ddot{\varphi} - m_3 L_1 \frac{\sin(\theta + \varphi)}{\cos(\varphi)} \ddot{x} \tag{4}$$

where a_{2_x} and a_{2_y} are the linear accelerations for the mass center of the connecting rod, $\ddot{\varphi}$ is the angular acceleration for the connecting rod, and $\ddot{x}$ is the linear acceleration for the piston. These kinematic properties will be presented in the following paragraphs.

Kinematic Analysis. For a constant shaft speed where $\dot{\theta} = \omega$, the geometry of Fig. 2 may be used to derive the linear accelerations for the mass center of the connecting rod as follows:

$$a_{2_x} = \ddot{x} + r_2 \cos(\varphi)\, \dot{\varphi}^2 + r_2 \sin(\varphi)\, \ddot{\varphi}$$
$$\text{and} \tag{5}$$
$$a_{2_y} = -r_2 \sin(\varphi)\, \dot{\varphi}^2 + r_2 \cos(\varphi)\, \ddot{\varphi}$$

Also, using Fig. 2, standard loop-closure methods may be used for describing the instantaneous position, velocity, and acceleration for the linkages of the single piston as it reciprocates within the internal combustion engine. These methods produce the following equations for the instantaneous linkage positions:

$$x = L_1 \cos(\theta) + L_2 \cos(\varphi) \quad \text{and} \quad 0 = L_1 \sin(\theta) - L_2 \sin(\varphi) \tag{6}$$

If we assume that θ is known, these two equations may be solved for x and φ. Similarly, the linkage velocities may be described using the following expressions:

$$\dot{x} = -L_1 \sin(\theta)\, \omega - L_2 \sin(\varphi)\, \dot{\varphi} \quad \text{and}$$
$$0 = L_1 \cos(\theta)\, \omega - L_2 \cos(\varphi)\, \dot{\varphi} \tag{7}$$

A simultaneous solution for these equations produces the following results for the linear velocity of the piston and the angular velocity of the connecting rod:

$$\dot{x} = -L_1 \frac{\sin(\theta + \varphi)}{\cos(\varphi)} \omega \quad \text{and} \quad \dot{\varphi} = \frac{L_1}{L_2} \frac{\cos(\theta)}{\cos(\varphi)} \omega \tag{8}$$

These results depend upon the solution for φ which may be obtained from Eq. (6). Again, it is assumed that θ and ω are known. Continuing with the loop-closure analysis, the linkage accelerations may be described as

$$\ddot{x} = -L_1 \cos(\theta)\, \omega^2 - L_2 \cos(\varphi)\, \dot{\varphi}^2 - L_2 \sin(\varphi)\, \ddot{\varphi}$$
$$\text{and} \tag{9}$$
$$0 = -L_1 \sin(\theta)\, \omega^2 + L_2 \sin(\varphi)\, \dot{\varphi}^2 - L_2 \cos(\varphi)\, \ddot{\varphi}$$

A simultaneous solution of these equations produces the following results for the linear acceleration of the piston and the angular acceleration of the connecting rod:

$$\ddot{x} = -L_1 \left(\cos(\theta) + \frac{L_1}{L_2} \frac{\cos^2(\theta)}{\cos^3(\varphi)} - \sin(\theta)\tan(\varphi) \right) \omega^2$$
$$\ddot{\varphi} = \frac{L_1}{L_2} \left(-\frac{\sin(\theta)}{\cos(\varphi)} + \frac{L_1}{L_2} \frac{\cos^2(\theta)}{\cos^2(\varphi)} \tan(\varphi) \right) \omega^2 \tag{10}$$

In the following paragraph, these equations will be nondimensionalized in order to provide the most general solutions possible with the fewest number of (nondimensional) parameters.

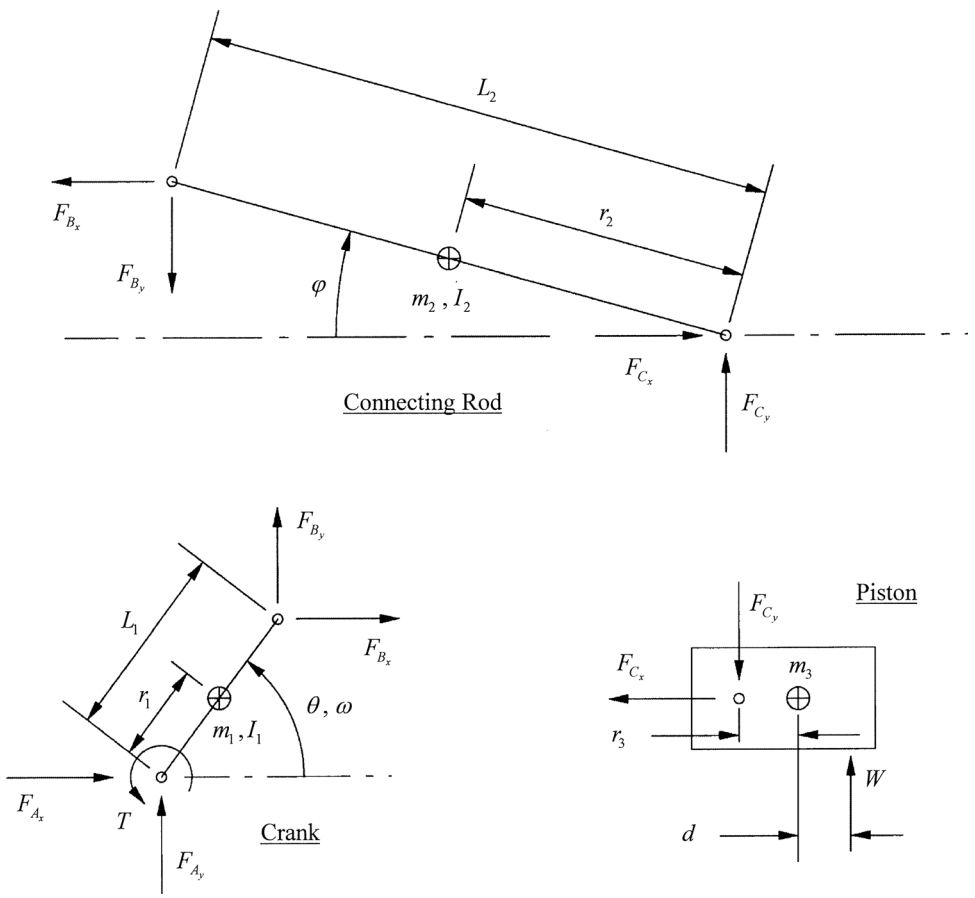

Fig. 3 Free-body diagrams for each linkage in the slider–crank mechanism

Nondimensional Analysis. In order to nondimensionalize the previous equations, the following definitions will be used:

$$
\begin{aligned}
&x = L_1\,\hat{x}, \quad L_2 = L_1\,\hat{L}_2, \quad r_2 = L_1\,\hat{r}_2, \quad t = \frac{\hat{t}}{\omega},\\
&a_{2_x} = L_1\,\omega^2\,\hat{a}_{2_x}, \quad a_{2_y} = L_1\,\omega^2\,\hat{a}_{2_y}, \quad \ddot{x} = L_1\,\omega^2\,\hat{\ddot{x}},\\
&\dot{\varphi} = \omega\,\hat{\dot{\varphi}}, \quad \ddot{\varphi} = \omega^2\,\hat{\ddot{\varphi}},\\
&m_2 = m_3\,\hat{m}_2, \quad I_2 = m_3 L_1^2\,\hat{I}_2, \quad T = m_3 L_1^2\,\omega^2\,\hat{T}
\end{aligned}
\tag{11}
$$

where the symbols with carets over the top are nondimensional and of order one. Using these definitions with the previous analysis, it may be shown that the nondimensional shaft torque is given by

$$
\begin{aligned}
\hat{T} = \hat{m}_2 &\left(-\left[\sin(\theta) + \left(1 - \frac{\hat{r}_2}{\hat{L}_2}\right)\cos(\theta)\tan(\varphi)\right]\hat{a}_{2_x} + \frac{\hat{r}_2}{\hat{L}_2}\cos(\theta)\hat{a}_{2_y}\right)\\
&+\hat{I}_2\frac{1}{\hat{L}_2}\frac{\cos(\theta)}{\cos(\varphi)}\hat{\ddot{\varphi}} - \frac{\sin(\theta+\varphi)}{\cos(\varphi)}\hat{\ddot{x}}
\end{aligned}
\tag{12}
$$

where the nondimensional acceleration properties are

$$
\begin{aligned}
&\hat{a}_{2_x} = \hat{\ddot{x}} + \hat{r}_2\,\cos(\varphi)\,\hat{\dot{\varphi}}^{\,2} + \hat{r}_2\,\sin(\varphi)\,\hat{\ddot{\varphi}},\\
&\hat{a}_{2_y} = -\hat{r}_2\,\sin(\varphi)\,\hat{\dot{\varphi}}^{\,2} + \hat{r}_2\,\cos(\varphi)\,\hat{\ddot{\varphi}},\\
&\hat{\dot{\varphi}} = \frac{1}{\hat{L}_2}\frac{\cos(\theta)}{\cos(\varphi)}, \quad \hat{\ddot{\varphi}} = -\frac{1}{\hat{L}_2}\frac{\sin(\theta)}{\cos(\varphi)} + \left(\frac{1}{\hat{L}_2}\frac{\cos(\theta)}{\cos(\varphi)}\right)^2\tan(\varphi),\\
&\hat{\ddot{x}} = -\cos(\theta) - \frac{1}{\hat{L}_2}\frac{\cos^2(\theta)}{\cos^3(\varphi)} + \sin(\theta)\tan(\varphi)
\end{aligned}
\tag{13}
$$

As shown in Eq. (12), the physical behavior of the crankshaft torque depends upon four nondimensional parameters: $\hat{m}_2$, $\hat{I}_2$, $\hat{L}_2$, and $\hat{r}_2$. It is instructive to note that all four of these parameters pertain to the design of the connecting rod.

Multiple Pistons. For an engine with multiple pistons that are evenly spaced in an angular direction about the centerline of the crankshaft, the angular position of the nth crank and the angular position of the nth connecting rod are given by

$$
\theta_n = \theta_1 + \frac{2\pi}{N}(n-1) \quad \text{and} \quad \varphi_n = \sin^{-1}\left[\frac{1}{\hat{L}_2}\,\sin(\theta_n)\right]
\tag{14}
$$

where θ_1 is the angular position of the first crank and N is the total number of pistons within the machine. By setting $\theta \to \theta_n$ and $\varphi \to \varphi_n$ in Eq. (12), the torque acting on the nth crank may be calculated as $\hat{T}_n$ and the total instantaneous torque on the crankshaft will be given by

$$
\hat{T}_T = \sum_{n=1}^{N}\hat{T}_n
\tag{15}
$$

Equation (15) produces an oscillating result with respect to the crank rotation θ_1 which describes the inertial imbalance of the engine. For all practical engine designs, it is impossible to eliminate this imbalance [4]; however, as will be shown in the Results section of this paper, there are certain engine designs that create a smaller torque imbalance than others. Generally speaking, engine designs with four or more pistons produce the smallest torque imbalance on the crankshaft.

Connecting-Rod Mass Approximations

An "Equivalent" System. As discussed in the literature review of this paper, it has become customary to avoid some of the complex analysis associated with the connecting rod by seeking to create an equivalent mass system that is shown in Fig. 4. This system replaces the actual connecting rod with a two-point mass system connected by a massless rod. In other words, the mass of the connecting rod is placed at the two ends of the connecting rod as noted in Fig. 4 by the symbols m_B and m_C. In order to consider these two systems as being equivalent, the following equations must be simultaneously satisfied [3]:

$$
\begin{aligned}
&\hat{m}_2 = \hat{m}_B + \hat{m}_C, \quad \hat{m}_B(\hat{L}_2 - \hat{r}_2) = \hat{m}_C\,\hat{r}_2,\\
&\hat{I}_2 = \hat{m}_B(\hat{L}_2 - \hat{r}_2)^2 + \hat{m}_C\,\hat{r}_2^2
\end{aligned}
\tag{16}
$$

where $m_B = m_3\,\hat{m}_B$ and $m_C = m_3\,\hat{m}_C$. The reader will recall that symbols with carets are nondimensional.

The first equation in Eq. (16) says that the total mass of the equivalent connecting rod must be equal to the total mass of the actual connecting rod. The second equation says that the mass center for the equivalent connecting rod must remain in the same location as the mass center of the actual connecting rod. The third equation says that mass moment-of-inertia about the mass center of the equivalent and the actual connecting rods must remain the same. Equation (16) represents three equations with only two unknowns given by $\hat{m}_B$ and $\hat{m}_C$. Customarily, the first two equations are the ones satisfied in the approximation, and the approximate mass moment-of-inertia is allowed to be generally different from that of the actual system [3]. In this case, the two-point masses are given by

$$
\hat{m}_B = \hat{m}_2\frac{\hat{r}_2}{\hat{L}_2} \quad \text{and} \quad \hat{m}_C = \hat{m}_2\left(1 - \frac{\hat{r}_2}{\hat{L}_2}\right)
\tag{17}
$$

Substituting these results into the third equations within Eq. (16) produces the following result for the approximate mass moment-of-inertia about the mass center of the connecting rod:

$$
\hat{I}_2' = \hat{m}_2(\hat{L}_2 - \hat{r}_2)\,\hat{r}_2
\tag{18}
$$

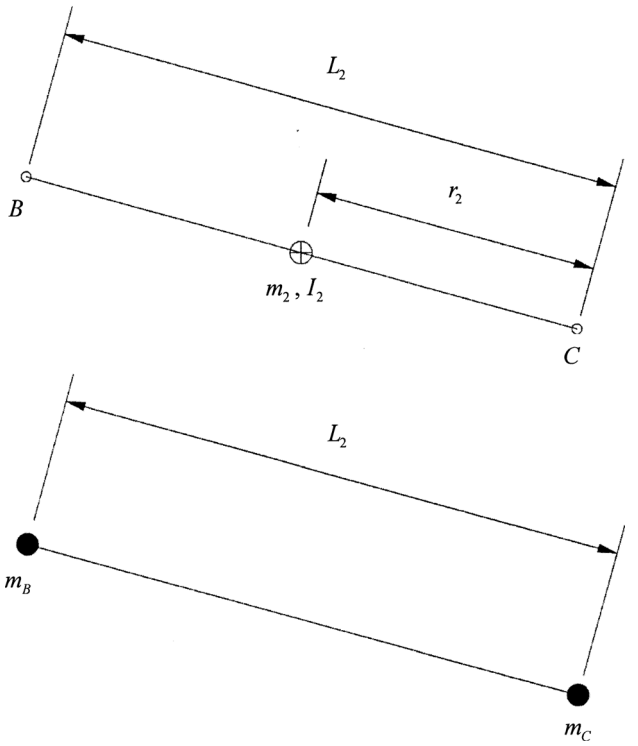

Fig. 4 The traditional mass approximation that is made for the connecting rod

which generally does not equal the mass moment-of-inertia for the actual system. Note: prime notation has been used to indicate that this moment-of-inertia describes the approximate system as opposed to the actual system.

Approximate Torque. To illustrate the motivation for using the mass approximation shown in Fig. 4, it may be shown that a substitution of $\hat{I}'_2$ for $\hat{I}_2$ in Eq. (12) produces the following result for the inertial torque acting on the crank:

$$\hat{T}' = \left(1 + \frac{\hat{I}'_2}{\hat{L}_2 \hat{r}_2}\right)\left(\frac{1}{\hat{L}_2}\frac{\cos^2(\theta)}{\cos^2(\varphi)} + \cos(\theta+\varphi)\right)\frac{\sin(\theta+\varphi)}{\cos^2(\varphi)} \tag{19}$$

This is a considerable simplification compared to the full result of Eq. (12). Again, the prime notation is used to indicate that this result is an approximation for the torque exerted on the crank, based upon the mass approximation shown in Fig. 4.

Multiple Pistons. Similar to the development of Eq. (15), an approximate total torque exerted on the crankshaft for an engine with multiple pistons may be calculated by setting $\theta \to \theta_n$ and $\varphi \to \varphi_n$ in Eq. (19), where θ_n and φ_n are given in Eq. (14). This produces a calculation for the approximate torque acting on the nth crank given by $\hat{T}'_n$. Using this result, the total instantaneous approximate-torque acting on the crankshaft may be calculated as

$$\hat{T}'_T = \sum_{n=1}^{N} \hat{T}'_n \tag{20}$$

This result will be used in the following paragraph to calculate an error between the total actual-torque and the total approximate-torque acting on the crankshaft.

Error Calculation. Part of this research is aimed at assessing the difference between the total actual-torque and the total approximate-torque acting on the crankshaft of the engine in order to validate the approximation method that is routinely presented in textbooks [1–4]. By assessing this error, we intend to describe the goodness of the mass approximation shown in Fig. 4 for engines with different numbers of pistons.

Before doing this, it is interesting to note that since the total mass of the connecting rod has remained unchanged in the approximation, the error between the actual and the approximate torque-imbalance for the internal combustion engine is based only on the difference between the actual and the approximate mass moment-of-inertia for the connecting rod, $\hat{I}_2 - \hat{I}'_2$. If there is no difference between the actual and the approximate mass moment-of-inertia for the connecting rod, then the error between the actual and the approximate torque imbalance vanishes and the approximation represents an exact solution. Using the previous analysis, a simple difference between the two torque calculations may be calculated as

$$\hat{T}_T - \hat{T}'_T = \sum_{n=1}^{N}\left(\hat{I}_2 - \hat{I}'_2\right)\frac{\left(1-\hat{L}_2^2\right)\cos(\theta_n)\sin(\theta_n)}{\left[\hat{L}_2^2 - \sin^2(\theta_n)\right]^2} \tag{21}$$

where θ_n is given in Eq. (14). This calculation is straightforward and simple, only depending upon the difference between the actual and the approximate mass moment-of-inertia, the length of the connecting rod $\hat{L}_2$, and the angular crank position of the first crank, θ_1.

In order to describe the goodness of the mass approximation shown in Fig. 4, we will employ the statistical measurement of the R^2 value which is also known as the coefficient of determination. This value is defined as

$$R^2 = 1 - \frac{\sum\left(\hat{T}_T - \hat{T}'_T\right)^2}{\sum\left(\hat{T}_T - 0\right)^2} \tag{22}$$

where the average torque imbalance on the crankshaft is shown by the numerical value of zero. The goodness of the approximation may be described as capturing a percentage of the variability of the actual torque imbalance about its mean, as calculated using the R^2 value. If the R^2 value is zero, then the mass approximation of Fig. 4 describes 0% of the variability of the actual torque imbalance about its mean, and the mass approximation of Fig. 4 is then considered to be a poor one. If the R^2 value is unity, then the mass approximation of Fig. 4 describes 100% of the variability of the actual torque imbalance about its mean, and the mass approximation is considered to be excellent. Percentages in between these two extremes are expected, and for the purposes of this research, we will consider R^2 values of 0.90 (90%) and above to indicate good approximations of the actual torque imbalance on the crankshaft.

Results and Discussion

Inertial Torque Imbalance. In order to evaluate the magnitude and frequency of the inertial torque imbalance, Eq. (12) was used to compute the nondimensional torque on the crank using the design parameters shown in the Appendix. This result is shown in Fig. 5 as the solid line for one revolution of a single-piston engine. The approximate result of Eq. (19) is also shown and will be discussed later. As shown in the figure, the torque imbalance is significant in magnitude with nondimensional values near unity. The reader will recall from the nondimensional definitions given in Eq. (11) that the torque result shown in Fig. 5 must be scaled by $m_3 L_1^2 \omega^2$ in order to consider its dimensional magnitude.

Figure 6 shows a fast Fourier transform (FFT) of Eq. (12) which is also plotted versus crank rotation in Fig. 5. From Fig. 6, it may be seen that the dominant frequency of the torque occurs at twice the crank speed but that there is frequency content at the first, third, and fourth harmonic as well. By neglecting the mass properties of the connecting rod, it may be shown that the dominant waveform of the second harmonic results from the cycle of accelerating and decelerating the piston during a single revolution.

While the single-piston engine is of interest, most internal combustion engines use multiple pistons within the same machine. The total inertial torque imbalance for these machines may be calculated using Eq. (15). Figure 7 shows these results for $N = 2, 3, \ldots, 6$. From this figure, it may be seen that the dominant frequency of torque oscillation during one revolution of the

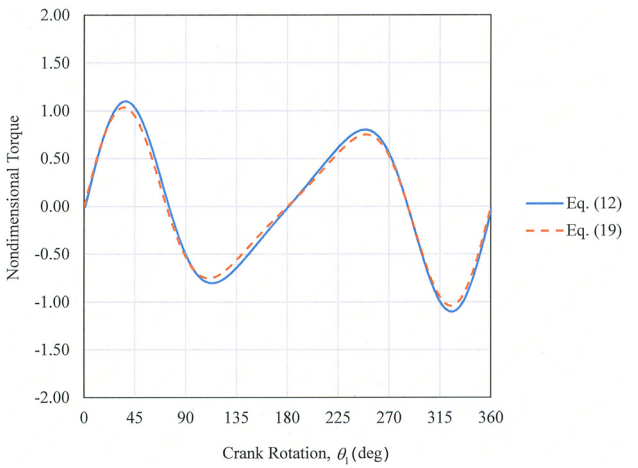

Fig. 5 Nondimensional torque on the crank for one revolution of a single-piston engine (scales match Fig. 7)

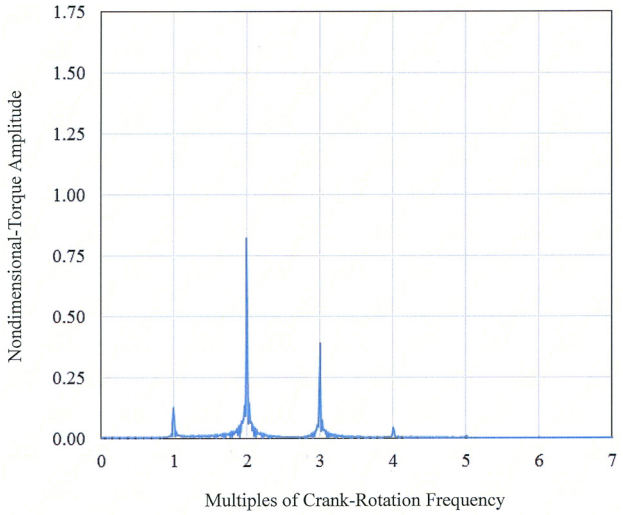

Fig. 6 Fast Fourier transform of the nondimensional torque on the crank of a single-piston engine (scales match Fig. 8)

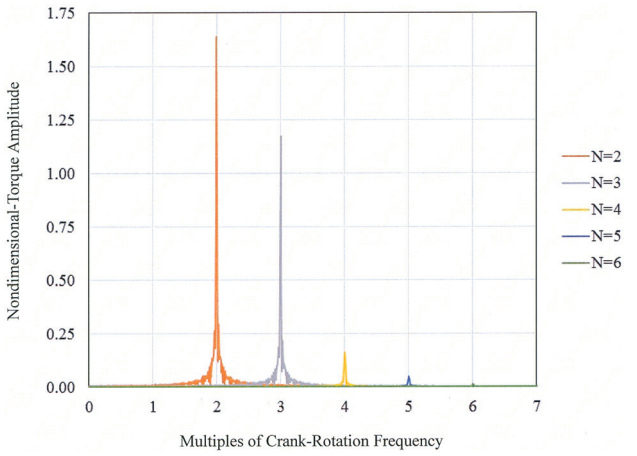

Fig. 8 Fast Fourier transform of the nondimensional torque on the crank of a multiple-piston engine (scales match Fig. 6)

machine is equal to the number of pistons in the machine. Furthermore, the amplitude of the torque oscillation is reduced as the number of pistons in the machine increases. It may also be seen from Fig. 7 that a dramatic reduction in the torque amplitude is realized when going from a three-piston engine to a four-piston engine. Although it is not shown in Fig. 7, the amplitude of torque oscillation for an eight-piston engine is essentially zero. Again, from the nondimensional definitions given in Eq. (11), the torque result shown in Fig. 7 must be scaled by $m_3 L_1^2 \omega^2$ in order to consider dimensional magnitudes.

Figure 8 shows a FFT of the torque results shown in Fig. 7, where the colors in each figure correspond with each other. From Fig. 8, it may be seen that for engines with a multiple number of pistons, the dominant frequency of the torque occurs at a frequency equal to the number of pistons in the machine times the crank speed. It turns out that there are really no other frequencies of importance. Recall, this is different compared to a single-piston engine where multiple harmonics of interest appeared. Comparing the amplitude scales for Figs. 6 and 8, it can be seen that the engine with the largest torque imbalance is a two-piston engine, followed by a three-piston engine, followed by a single-piston engine (not monotonic). As shown in the FFT plot of Fig. 8, a dramatic reduction in the torque imbalance is observed when changing from a three-piston engine to a four-piston engine. Engines with five pistons and higher observe a negligible torque imbalance on the crankshaft. It is also important to note that the piston assemblies within each engine are identical in size, meaning that the two-piston engine is twice the displacement of the single-piston engine. This, however, does not alter the scale factor that needs to be multiplied by each amplitude in order to consider the dimensional torque. That scale factor is still $m_3 L_1^2 \omega^2$.

Mass Approximation. As previously discussed, the R^2 value has been used in this research to assess the goodness of the mass approximation for the connecting rod as shown in Fig. 4. This approximation is customarily used in machine design textbooks, but without an argument for justifying its use or assessing the goodness of the approximation. We present here, for the first time known to the authors, a comparison between the actual and the approximate calculations for the inertial torque imbalance within an internal combustion engine. This comparison is shown in Fig. 9.

As shown in Fig. 9, the R^2 values for the approximate calculations of the inertial torque imbalance are all greater than 0.98, which means that the mass approximation of Fig. 4 captures more than 98% of the variability of the actual torque imbalance about its mean. In addition, it should be observed that the mass approximation captures 100% of the variability of the actual torque imbalance for engines that are designed with an odd number of

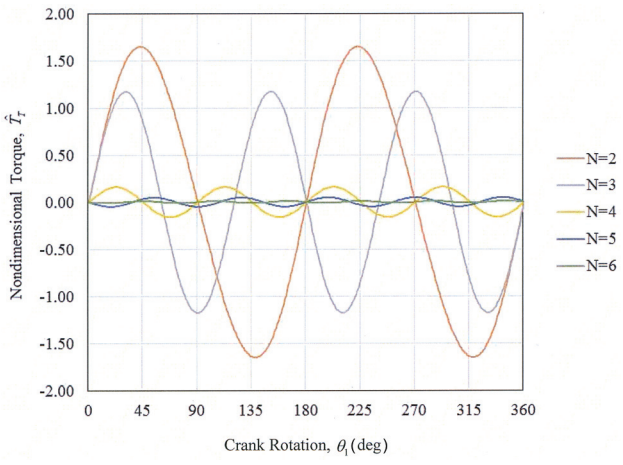

Fig. 7 Nondimensional torque on the crank for one revolution of a multiple-piston engine (scales match Fig. 5)

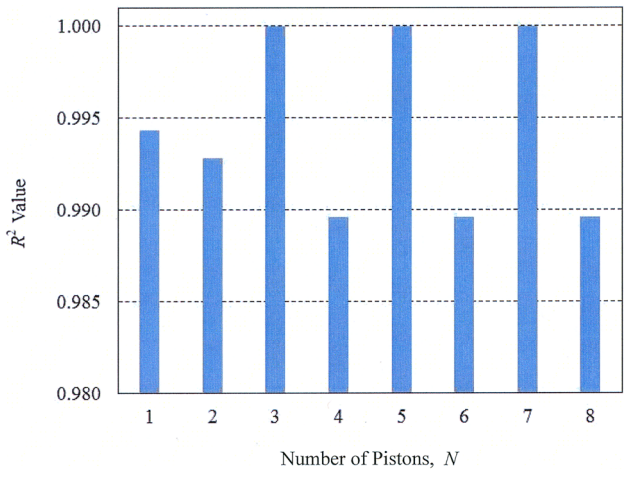

Fig. 9 R^2 values for the approximate calculation of the inertial torque imbalance, i.e., a statistical comparison for Eqs. (15) and (20)

pistons equal to or greater than three. In other words, there are cases where the mass approximation is not an approximation at all—it is essentially exact. The conclusion to be drawn from this analysis is that the mass approximation of Fig. 4 is very good and that it should be generally used with confidence. These results have been generated using the values in the Appendix, which the authors believe are typical of most practical designs for internal combustion engines.

Conclusion

The following conclusions are supported by the analysis, results, and discussion of this paper:

(1) That an internal combustion engine using a single piston exhibits a torque imbalance with harmonic content at four different multiples of the crank-rotation frequency.
(2) That the largest torque imbalance is exhibited by a two-piston engine. The next largest torque imbalance is exhibited by a three-piston engine, followed by a single-piston engine (this is not monotonic).
(3) That an internal combustion engine using 1, 2, or 3 pistons produces an inertial-torque imbalance on the dimensional order of $m_3 L_1^2 \omega^2$, where each symbol is defined in the Nomenclature section of this paper. Note: as shown by this scale factor, this torque imbalance increases with the square of the crank speed ω.
(4) That a dramatic reduction in the torque imbalance may be obtained by using four or more pistons in the design, and when using as many as eight pistons, the torque imbalance essentially vanishes.
(5) That the customary mass approximation shown in Fig. 4 does an excellent job of capturing the variability of the actual torque imbalance about its mean and should therefore be used with confidence.

In summary, this paper has shown that there is merit in using four or more pistons in the internal combustion engine for the purpose of reducing the inertial-torque imbalance. Furthermore, this research has analytically and numerically verified that the approximate torque calculation shown in Eq. (19) may be used in preference to the more complicated calculation shown in Eq. (12) without a significant loss of accuracy.

Nomenclature

a_{1_x} = linear acceleration in the x-direction of the crank mass-center
a_{1_y} = linear acceleration in the y-direction of the crank mass-center
a_{2_x} = linear acceleration in the x-direction of the connecting rod mass-center
a_{2_y} = linear acceleration in the y-direction of the connecting rod mass-center
d = location of the reaction force between the piston and the cylinder wall
F_{A_x} = reaction force between the ground and the crank in the x-direction
F_{A_y} = reaction force between the ground and the crank in the y-direction
F_{B_x} = reaction force between the crank and the connecting rod in the x-direction
F_{B_y} = reaction force between the crank and the connecting rod in the y-direction
F_{C_x} = reaction force between the connecting rod and the piston in the x-direction
F_{C_y} = reaction force between the connecting rod and the piston in the y-direction
I_1 = mass moment-of-inertia of the crank about its mass center
I_2 = mass moment-of-inertia of the connecting rod about its mass center
L_1 = length of the crank
L_2 = length of the connecting rod
m_B = point mass at B for the approximate connecting rod
m_C = point mass at C for the approximate connecting rod
m_1 = mass of the crank
m_2 = mass of the connecting rod
m_3 = mass of the piston
r_1 = location of the mass center for the crank
r_2 = location of the mass center for the connecting rod
r_3 = location of the mass center for the piston
T = torque on the crank from a single piston
T_T = total torque on the crankshaft from multiple pistons
W = reaction force between the piston and the cylinder wall
x = instantaneous displacement of the piston
θ = angular displacement of the crank
φ = angular displacement of the connecting rod
ω = angular velocity of the crank

Appendix

The following design parameters were used to generate the results of this research:

$\hat{m}_2 = 1, \hat{I}_2 = 1, \hat{L}_2 = 3$, and $\hat{r}_2 = 3/2$.

References

[1] Norton, R. L., 2012, *Design of Machinery: An Introduction to the Synthesis and Analysis of Mechanisms and Machines*, 5th ed., McGraw-Hill, New York.
[2] Uicker, J. J., Pennock, G. R., and Shigley, J. E., 2003, *Theory of Machines and Mechanisms*, Oxford University Press, New York.
[3] Wilson, C. E., and Sadler, J. P., 2003, *Kinematics and Dynamics of Machinery*, 3rd ed., Pearson Education, Upper Saddle River, NJ.
[4] Timoshenko, S., and Young, D. H., 1948, *Advanced Dynamics*, McGraw-Hill, New York.
[5] Meirovitch, L., 1986, *Elements of Vibration Analysis*, 2nd ed., McGraw-Hill, New York.
[6] Dimarogonas, A. D., and Paipetis, S. A., 1983, *Analytical Methods in Rotor Dynamics*, Applied Science Publishers, London.
[7] Dimarogonas, A. D., 1976, *Vibration Engineering*, West Publishing, New York.
[8] Li, P., Shen, T., and Liu, D., 2012, "Idle Speed Performance Improvement Via Torque Balancing Control in Ignition-Event Scale for SI Engines With Multi-Cylinders," Int. J. Engine Res., **13**(1), pp. 65–76.
[9] Osburn, A. W., and Franchek, M. A., 2006, "Reducing Engine Idle Speed Deviations Using the Internal Model Principle," ASME J. Dyn. Syst. Meas. Control, **128**(4), pp. 869–877.
[10] Arakelian, V., and Briot, S., 2010, "Simultaneous Inertia Force/Moment Balancing and Torque Compensation of Slider-Crank Mechanisms," Mech. Res. Commun., **37**(2), pp. 265–269.
[11] Bagci, C., 1995, "A Simplified Approach for Balancing of Multi-Cylinder Engines," 13th International Modal Analysis Conference, Nashville, TN, Feb. 13–16, pp. 879–884.